Continuous layer gap plasmon resonators

Michael G. Nielsen,[1,*] Dmitri K. Gramotnev,[1,2] Anders Pors,[3] Ole Albrektsen,[1] and Sergey I. Bozhevolnyi[1]

[1]*Institute of Technology and Innovation (ITI), University of Southern Denmark, Niels Bohrs Allé 1, DK-5230 Odense M, Denmark*
[2]*Nanophotonics, GPO Box 786, Albany Creek, Queensland 4035, Australia*
[3]*Mads Clausen Institute (MCI), University of Southern Denmark, Alsion 2, DK-6400 Sønderborg, Denmark*
[*]*mgni@iti.sdu.dk*

Abstract: We demonstrate both theoretically and experimentally that a gold nanostrip supported by a thin dielectric (silicon dioxide) film and a gold underlay forms an efficient (Fabry-Perot) resonator for gap surface plasmons. Periodic nanostrip arrays are shown to exhibit strong and narrow resonances with nearly complete absorption and quality factors of ~15-20 in the near-infrared. Two-photon luminescence microscopy measurements reveal intensity enhancement factors of ~120 in the 400-nm-period array of 85-nm-wide gold strips atop a 23-nm-thick silica film at the resonance wavelength of ~770nm. Excellent resonant characteristics, the simplicity of tuning the resonance wavelength by adjusting the nanostrip width and/or the dielectric film thickness and the ease of fabrication with (only) one lithography step required make the considered plasmonic configuration very attractive for a wide variety of applications, ranging from surface sensing to photovoltaics.

OCIS codes: (250.5403) Plasmonics; (240.6680) Surface plasmons; (260.3910) Metal optics; (190.0190) Nonlinear optics; (300.1030) Absorption; (040.5350) Photovoltaic.

References and links

1. L. Novotny and B. Hecht, "Principles of Nano-Optics," Cambridge University Press, Cambridge, (2006).
2. W. Zhang, L. Huang, C. Santschi, and O. J. F. Martin, "Trapping and sensing 10 nm metal nanoparticles using plasmonic dipole antennas," Nano Lett. **10**(3), 1006–1011 (2010).
3. M. L. Juan, M. Righini, and R. Quidant, "Plasmon nano-optical tweezers," Nat. Photonics **5**(6), 349–356 (2011).
4. A. Weber-Bargioni, A. Schwartzberg, M. Schmidt, B. Harteneck, D. F. Ogletree, P. J. Schuck, and S. Cabrini, "Functional plasmonic antenna scanning probes fabricated by induced-deposition mask lithography," Nanotechnology **21**(6), 065306 (2010).
5. J. N. Farahani, D. W. Pohl, H.-J. Eisler, and B. Hecht, "Single quantum dot coupled to a scanning optical antenna: a tunable superemitter," Phys. Rev. Lett. **95**(1), 017402 (2005).
6. H. A. Atwater and A. Polman, "Plasmonics for improved photovoltaic devices," Nat. Mater. **9**(3), 205–213 (2010).
7. L. Tang, S. Latif, A. K. Okyay, D.-S. Ly-Gagnon, K. C. Saraswat, and D. A. B. Miller, "Nanometre-scale germanium photodetector enhanced by a near-infrared dipole antenna," Nat. Photonics **2**(4), 226–229 (2008).
8. J. A. Schuller, E. S. Barnard, W. Cai, Y. C. Jun, J. S. White, and M. L. Brongersma, "Plasmonics for extreme light concentration and manipulation," Nat. Mater. **9**(3), 193–204 (2010).
9. P. Bharadwaj, B. Deutsch, and L. Novotny, "Optical antennas," Adv. Opt. Photon. **1**(3), 438–483 (2009).
10. L. Novotny and N. Van Hulst, "Antennas for light," Nat. Photonics **5**(2), 83–90 (2011).
11. D. K. Gramotnev and S. I. Bozhevolnyi, "Plasmonics beyond the diffraction limit," Nat. Photonics **4**(2), 83–91 (2010).
12. A. Kinkhabwala, Z. Yu, S. Fan, Y. Avlasevich, K. Mullen, and W. E. Moerner, "Large single-molecule fluorescence enhancements produced by bowtie nanoantenna," Nat. Photonics **3**(11), 654–657 (2009).
13. T. Søndergaard and S. I. Bozhevolnyi, "Slow-plasmon resonant nanostructures: Scattering and field enhancements," Phys. Rev. B **75**(7), 073402 (2007).
14. S. I. Bozhevolnyi and T. Søndergaard, "General properties of slow-plasmon resonant nanostructures: Nano-antennas and resonators," Opt. Express **15**(17), 10869–10877 (2007).
15. T. Søndergaard and S. I. Bozhevolnyi, "Metal nano-strip optical resonators," Opt. Express **15**(7), 4198–4204 (2007).

#151634 - $15.00 USD Received 26 Jul 2011; revised 25 Aug 2011; accepted 7 Sep 2011; published 20 Sep 2011

16. T. Søndergaard and S. I. Bozhevolnyi, "Strip and gap plasmon polariton optical resonators," Phys. Stat. Solidi B **245**(1), 9–19 (2008).
17. T. Søndergaard, J. Beermann, A. Boltasseva, and S. I. Bozhevolnyi, "Slow-plasmon resonant-nanostrip antennas: Analysis and demonstration," Phys. Rev. B **77**(11), 115420 (2008).
18. J. Jung, T. Søndergaard, and S. I. Bozhevolnyi, "Gap plasmon-polariton nanoresonators: Scattering enhancement and launching of surface plasmon polaritons," Phys. Rev. B **79**(3), 035401 (2009).
19. J. Jung, T. Søndergaard, J. Beermann, A. Boltasseva, and S. I. Bozhevolnyi, "Theoretical analysis and experimental demonstration of resonant light scattering from metal nanostrips on quartz," J. Opt. Soc. Am. B **26**(1), 121–124 (2009).
20. H. T. Miyazaki and Y. Kurokawa, "Squeezing visible light waves into a 3-nm-thick and 55-nm-long plasmon cavity," Phys. Rev. Lett. **96**(9), 097401 (2006).
21. P. Bouchon, F. Pardo, B. Portier, L. Ferlazzo, P. Ghenuche, G. Dagher, C. Dupuis, N. Bardou, R. Haidar, and J.-L. Pelouard, "Total funneling of light in high aspect ratio plasmonic nanoresonators," Appl. Phys. Lett. **98**(19), 191109 (2011).
22. T. Søndergaard, J. Jung, S. I. Bozhevolnyi, and G. D. Valle, "Theoretical analysis of gold nanostrip gap plasmon resonators," N. J. Phys. **10**(10), 105008 (2008).
23. G. Lerosey, D. F. P. Pile, P. Matheu, G. Bartal, and X. Zhang, "Controlling the phase and amplitude of plasmon sources at a subwavelength scale," Nano Lett. **9**(1), 327–331 (2009).
24. G. Lévêque and O. J. F. Martin, "Tunable composite nanoparticle for plasmonics," Opt. Lett. **31**(18), 2750–2752 (2006).
25. Y. Chu and K. B. Crozier, "Experimental study of the interaction between localized and propagating surface plasmons," Opt. Lett. **34**(3), 244–246 (2009).
26. Y. Chu, M. G. Banaee, and K. B. Crozier, "Double-resonance plasmon substrates for surface-enhanced Raman scattering with enhancement at excitation and stokes frequencies," ACS Nano **4**(5), 2804–2810 (2010).
27. R. Ameling, D. Dregely, and H. Giessen, "Strong coupling of localized and surface plasmons to microcavity modes," Opt. Lett. **36**(12), 2218–2220 (2011).
28. S. H. Lim, W. Mar, P. Matheu, D. Derkacs, and E. T. Yu, "Photocurrent spectroscopy of optical absorption enhancement in silicon photodiodes via scattering from surface plasmon polaritons in gold nanoparticles," J. Appl. Phys. **101**(10), 104309 (2007).
29. P. B. Johnson and R. W. Christy, "Optical constants of the noble metals," Phys. Rev. B **6**(12), 4370–4379 (1972).
30. J. Jin, "The finite element method in electromagnetics," Wiley: New York, p 429 (1993).
31. F. Wang and Y. R. Shen, "General properties of local plasmons in metal nanostructures," Phys. Rev. Lett. **97**(20), 206806 (2006).
32. J. Beermann, S. M. Novikov, T. Søndergaard, A. E. Boltasseva, and S. I. Bozhevolnyi, "Two-photon mapping of localized field enhancements in thin nanostrip antennas," Opt. Express **16**(22), 17302–17309 (2008).
33. M. G. Nielsen, A. Pors, R. B. Nielsen, A. Boltasseva, O. Albrektsen, and S. I. Bozhevolnyi, "Demonstration of scattering suppression in retardation-based plasmonic nanoantennas," Opt. Express **18**(14), 14802–14811 (2010).
34. J. Beermann, I. P. Radko, A. Boltasseva, and S. I. Bozhevolnyi, "Localized field enhancements in fractal shaped periodic metal nanostructures," Opt. Express **15**(23), 15234–15241 (2007).
35. J. Beermann, A. Evlyukhin, A. Boltasseva, and S. I. Bozhevolnyi, "Nonlinear microscopy of localized field enhancements in fractal shaped periodic metal nanostructures," J. Opt. Soc. Am. B **25**(10), 1585–1592 (2008).
36. J. Beermann, T. Søndergaard, S. M. Novikov, S. I. Bozhevolnyi, E. Devaux, and T. W. Ebbesen, "Field enhancement and extraordinary optical transmission by tapered periodic slits in gold films," N. J. Phys. **13**(6), 063029 (2011).
37. P. J. Schuck, D. P. Fromm, A. Sundaramurthy, G. S. Kino, and W. E. Moerner, "Improving the mismatch between light and nanoscale objects with gold bowtie nanoantennas," Phys. Rev. Lett. **94**(1), 017402 (2005).

1. Introduction

Subwavelength confinement and enhancement of light in metallic nanostructures due to resonant excitation of surface plasmon polaritons is a rapidly growing research direction in nano-optics and nanophotonics with the major focus onto the development of new efficient approaches for the delivery of light energy to nanoscale objects and single molecules [1]. This is because of the unique opportunities offered by plasmonic subwavelength resonators for the design of plasmonic nanosensors, nanomanipulation and near-field trapping techniques [2, 3], high-resolution probes for nanoimaging and new information processing approaches [4, 5], improved photovoltaics [6], nanoscale photodetectors with significantly enhanced signal-to-noise ratio [7, 8], catalysis applications [8], efficient coupling of light energy to nanoscale structures, quantum dots and single molecules [9–11]. Plasmonic resonators are also expected to result in observation and applications of highly localized and enhanced non-linear effects and near-field spectroscopy, including spectroscopic analysis, imaging and identification of nanoscale amounts of substances and single molecules [8–12].

#151634 - $15.00 USD Received 26 Jul 2011; revised 25 Aug 2011; accepted 7 Sep 2011; published 20 Sep 2011

In this respect, special interest present the retardation-based resonant nanostructures [13], which are realized by truncating the metal-insulator-metal (MIM) or insulator-metal-insulator (IMI) configurations to achieve multiple reflections of (slow) surface plasmon-polariton modes (gap and short-range surface plasmon modes, respectively) from the terminations (edges) of the obtained structures, similar to a conventional Fabry-Perot resonator [13–19]. The comparative analysis of plasmonic IMI and MIM nanoresonators has revealed significant radiative losses from the former due to large electric dipole moments associated with the fundamental resonance modes [14]. Significant advantages of MIM resonators involving gap surface plasmons (GSPs), as compared to IMI nanostrip resonators, were demonstrated [20,21] and analyzed theoretically [16,22]. Quality factors up to ~20 were predicted for such GSP-based resonators [23].

Theoretical studies of gap plasmon resonators (GPRs) have so far been mainly confined to the structures where the same truncation was carried out for *more* than one layer in a MIM structure [16, 22–24]. Meanwhile, it has been pointed out that a finite-width metal strip placed close to a metal surface does ensure efficient reflection of GSPs at strip terminations, forming an efficient GPR [18]. One might pursue further this idea by exploring plasmonic configurations, in which finite-size metal patches/strips are placed on a thin dielectric layer supported by a metal underlay (or by a thick metal film atop a substrate). It seems reasonable to expect that such a structure (whose fabrication requires only one lithographic step) would exhibit retardation (Fabry-Perot) resonances due to multiple reflections of GSPs. In fact, numerical and experimental investigations of plasmonic nanoresonators in the form of metal nanodisks on a continuous thin dielectric film on a metal underlay have recently been reported [25, 26], but no evidence or analysis of the contribution of GSPs and retardation to the observed resonances has been presented. The obtained results have only been investigated and interpreted under the assumption of the quasistatic resonance in the disk, red-shifted by the near-field interaction between the gold nanodisk and its electrostatic image in the metal substrate (thick gold underlay) [25, 26]. Another very recent paper has considered plasmonic resonators in the form of gold strips forming a periodic array on a continuous thin dielectric layer on a gold underlay [27]. However, the analysis in this paper was rather focused onto the interaction of these structures with an additional microcavity formed by two microscopically separated mirrors [27]. The analysis of the strip resonators themselves, their excitation by an incident bulk wave (including absorption and scattering cross-sections), typical local field enhancements, achievable Q-factors, and the retardation nature of the resonances, related to the GSP generation and multiple reflection at strip terminations, has so far been left out. This leaves major gaps in the current physical understanding of GPRs and their potential applications.

In this paper, we introduce and investigate, both theoretically and experimentally, a simple plasmonic resonant structure termed a continuous layer gap plasmon resonator (CL-GPR), for which nanoscale truncation is carried out only for the *top* layer in a MIM structure (that can be achieved by only a single lithographic step). Spatial extension of the considered GSPs is defined by the width of a metal strip fabricated on a (thin) continuous dielectric layer supported by an underlying thick metal film (underlay). Arrays of CL-GPRs are fabricated and analyzed for different periods and widths of the metal strips featuring strong and narrow resonances. We demonstrate that the predicted and observed resonances occur due to GSPs experiencing multiple reflections from the edges of each of the metal strips.

2. Structure and numerical methods

The considered CL-GPR structure consists of a continuous SiO_2 film ($n_d = 1.45$) of thickness t sandwiched between a 200nm-thick continuous gold underlay and a gold nanostrip of height h and width w (Fig. 1). The cladding above the structure is assumed to be air ($n = 1$), and the CL-GPR structure is uniform along the z-direction (Fig. 1). The physical principles for the considered resonator structures are similar to those of a conventional Fabry-Perot resonator. The GSP guided by the gap (filled with SiO_2) between the metal strip and the underlay experiences multiple reflections from the terminations (edges) of the strip. The radiation

#151634 - $15.00 USD Received 26 Jul 2011; revised 25 Aug 2011; accepted 7 Sep 2011; published 20 Sep 2011

losses at the edges of the strip are due to electric dipole radiation caused by the oscillating opposite charges across the gap. However, because the size of this electric dipole moment is ~t (i.e., in tens of nanometers - much smaller than the wavelength), these radiation losses are significantly weaker than those in the case of the metal strip (IMI) resonator [17]. As a result, the typical Q-factors of CL-GPR are expected to be significantly higher than for the IMI resonators.

To model the resonator's optical response, we use the finite-element method (FEM) implemented in the commercial software COMSOL MULTIPHYSICS, and consider a monochromatic plane wave with the amplitude E_0, polarized along the x-axis (TM-wave) and incident normally onto the CL-GPR structure (Fig. 1). The perfect electric conductor boundary conditions are applied to the unit-cell side walls, thereby mimicking structural periodicity in the x-direction [28]. The corners of the gold nanostrip are assumed to be rounded with the radius 5nm, and the permittivity of gold is described by a complex-valued frequency-dependent dielectric function $\varepsilon_m(\omega)$ *obtained by the cubic interpolation* of the tabular values [29]. The CL-GPR reflectivity is calculated as a function of wavelength by integrating the Poynting vector along a first-order absorption boundary [30] also generating the incident wave and positioned at 800nm above the gold underlay. The calculated reflectivity is normalized to the reflectivity from a uniform smooth gold surface with the thin SiO_2 layer. The accuracy and validity of the obtained results were also confirmed by using a perfectly matched layer, instead of the first-order absorption boundary, to suppress the artificial reflections.

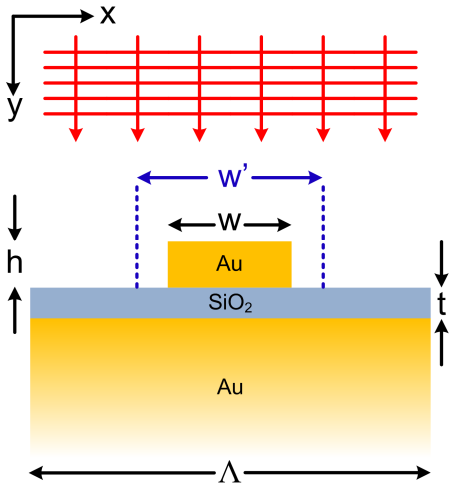

Fig. 1. The configuration of a CL-GPR unit-cell. A continuous SiO_2 film with the thickness t is sandwiched between a continuous 200nm thick gold underlay and a gold strip with the height h and width w; the vertical dashed lines indicate the effective resonator length $w' > w$, caused by an additional plasmon phase shift acquired by the GSP upon reflection from an edge of the metal strip. The domain above the SiO_2 film is assumed to be air. The CL-GPR unit-cell is periodically repeated along the x-axis with period Λ. A plane wave is incident normally onto the structure (along the y-direction) and is polarized along the x-axis (TM polarization).

3. Reflectivity dependence on structural parameters

Figure 2(a) and Fig. 2(b) show the numerical dependences of the reflectivity from a periodic array of gold nanostrips forming an array of CL-GPRs with fixed h = 50nm and w = 85nm, two different structural periods Λ = 400nm [Fig. 2(a)] and Λ = 600nm [Fig. 2(b)], and four indicated thicknesses t of the SiO_2 layer. The major feature of all the curves presented in Fig. 2(a) and Fig. 2(b) is the display of the strongly resonant behavior between ~650 nm and ~850 nm. This behavior is especially evident and strong at smaller thicknesses of the SiO_2 layer. This is because the gaps of smaller thicknesses must result in weaker radiation losses at the

#151634 - $15.00 USD Received 26 Jul 2011; revised 25 Aug 2011; accepted 7 Sep 2011; published 20 Sep 2011

terminations of the strips (due to smaller dimensions of the radiating electric dipoles - see above). Quite remarkably, the reflectivity from the periodic CL-GPR arrays on a SiO_2 layer of ~10nm thickness is almost zero at the resonant wavelengths [Fig. 2(a,b)], which means that practically all of the incident energy in the plane wave is efficiently coupled into the CL-GPR modes and dissipates in the metal. Furthermore, the resonant wavelengths at which the reflectivity is nearly zero [Fig. 2(a,b)] are far from the resonances associated with the surface plasmon excitation in the structure (i.e., from the conventional grating resonances). This means that the predicted resonances are indeed related to the GSPs generated by the incident radiation in the gaps under the gold strips. As expected, resonant generation of surface plasmons (grating resonances) can only be observed in Fig. 2(b) at the wavelengths of ~600nm for the CL-GPR array period Λ = 600nm. The smaller period Λ = 400nm expectedly does not lead to such grating resonances [Fig. 2(a)], as surface plasmons with such wavelength do not exist on a gold-vacuum surface (including with the considered SiO_2 layer).

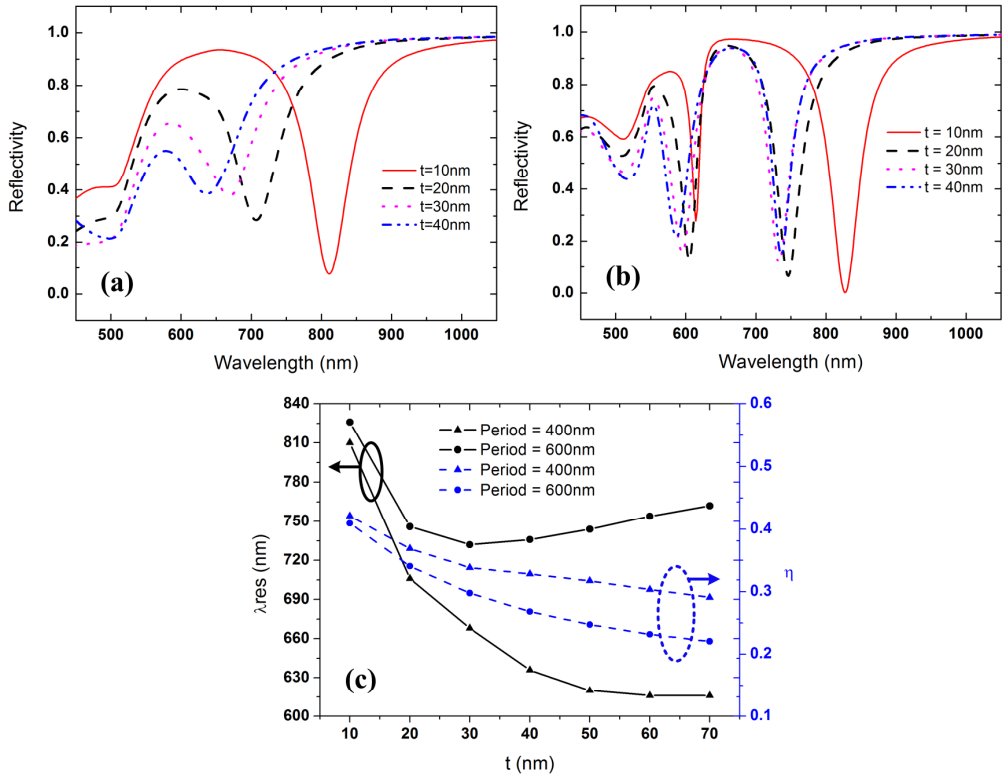

Fig. 2. (a,b) Reflectivity spectra with t as a parameter for the two different CL-GPR array periods: (a) Λ = 400nm and (b) Λ = 600nm; w = 85nm. (c) The dependences of the GSP resonance wavelength (solid curves) and the parameter n (dashed curves) determining the additional phase shift of the GSPs upon their reflection from the edges of the gold strip on thickness t of the SiO_2 layer.

Figure 2(a) also demonstrates that decreasing thickness t of the SiO_2 layer results in increasing resonant wavelength. This can be regarded as further confirmation that the predicted resonances are caused by GSPs between the gold strips and gold underlay, because decreasing thickness of the SiO_2 layer (gap width) results in decreasing GSP wavelength, i.e., increasing vacuum wavelength corresponding to the fundamental resonance at a fixed width of the gold strip. However, this simple trend of increasing resonant wavelength with decreasing t does not seem to hold well at larger thicknesses of the SiO_2 layer [solid curves in Fig. 2 (c)]. For example, for the CL-GPR array with the period Λ = 400nm [the lower solid curve in Fig. 2(c)], the resonant wavelength tends to be approximately constant for the SiO_2

#151634 - $15.00 USD Received 26 Jul 2011; revised 25 Aug 2011; accepted 7 Sep 2011; published 20 Sep 2011

thicknesses t > 50nm. Furthermore, for the CL-GPR array with the period Λ = 600nm [the upper solid curve in Fig. 2 (c)], the resonant wavelength tends to increase (the resonance is redshifted) for t > 30 nm. This observed behavior of the resonant wavelength can be explained as follows.

The resonance condition for CL-GPR can be written as for any other Fabry-Perot-type resonator:

$$w\frac{2\pi}{\lambda}n_{gsp} = m\pi - \varphi, \tag{1}$$

where λ is the free-space wavelength, n_{gsp} is the effective index for the GSP, m is an integer determining the order of a resonance mode, and φ is the phase acquired by the GSP upon its reflection at the resonator terminations (edges of the strip). Considering only the fundamental mode (m = 1) and defining the phase parameter $\eta = \frac{1}{2}(1-\varphi/\pi)$, Eq. (1) can be rearranged as:

$$w \cdot n_{gsp} = \lambda\eta. \tag{2}$$

If the phase shift φ is zero, then η = 1/2 (like for a perfectly conducting mirror). However, reflection of a GSP from the terminations of a metal strip in the geometry shown in Fig. 1 is associated with a non-zero phase shift φ *that depends upon the structural and material parameters. The physical explanation for this non-zero phase shift* φ is related to extension of the plasmon field beyond the edges of the metal strip. As a result, it can be regarded that plasmon reflections effectively occur not from the edges of the strip, but rather from some 'effective boundaries' of CL-GPR, indicated by the dashed vertical lines in Fig. 1. The dashed curves in Fig. 2(c) show the calculated dependences of η on thickness t of the SiO_2 layer. It can be seen that, for both the considered periods of the CL-GPR arrays, the phase parameter η monotonically decreases from ~0.4 to ~0.2 - 0.3 with increasing t from 10nm to 70nm. This is because, as the gap width (thickness of the SiO_2 layer) increases, the GSP propagation constant decreases and becomes closer to that of the bulk wave in the air, which causes the plasmonic field to extend further beyond the edges of the gold strip, thus decreasing η [dashed curves in Fig. 2(c)] or, in other words, moving further away from the limiting case of perfect mirrors with η = 1/2.

The comparison of the curves in Fig. 2(c) suggests that the additional phase shift also depends on period of the CL-GPR array, affecting thereby the effective resonator length w'. It is seen that the additional phase shift and effective resonator length w' are larger for a larger period (Λ = 600nm) than those for Λ = 400nm [Fig. 2(c)]. There are two possible mechanisms that could contribute to this behavior. Firstly, this could be related to interaction between CL-GPRs and the grating plasmonic resonance (the Rayleigh anomaly). If the grating resonance is absent [Fig. 2(a)], the resonant wavelength for CL-GPRs monotonically decrease with increasing t [Fig. 2(a,c)]. If the array period is increased to 600nm, grating resonances appear at ~600nm [Fig. 2(b)]. In this case, if t is small [e.g., t = 10nm - the solid curve in Fig. 2(b)], then the CL-GPR resonance and the grating resonance are sufficiently far apart, so that they do not interact, and the resonant wavelength decreases with increasing t [Fig. 2(b,c)]. However, further increase of t shifts the CL-GPR resonance closer towards the grating resonance [Fig. 2(b)], and these two resonances may start interacting (similar to the case of metallic nanodisk resonators [25, 26]). As a result, the effective resonator length w' may significantly increase [and η decrease - dashed curves in Fig. 2(c)]. It is nevertheless, questionable if the described interaction is indeed significant for the resonances shown in Fig. 2(b), as they seem to be too separated for such an interaction to effectively take place. Therefore, the second possible mechanism that could explain the unusual dependence of w'

#151634 - $15.00 USD Received 26 Jul 2011; revised 25 Aug 2011; accepted 7 Sep 2011; published 20 Sep 2011

(and n) on period of the CL-GPR array is the interaction (coupling) between the neighboring CL-GPRs by means of the generated surface plasmons. GSPs under the gold strips are expected to leak not only into bulk waves in the air, but also into the surface plasmons propagating in the gaps between CL-GPRs. These surface plasmons may result in efficient radiative coupling between the CL-GPR cavities. Because this type of coupling should heavily rely upon the interference effects involving the surface plasmons between the CL-GPR cavities, the coupling efficiency is expected to significantly vary with changing array period. If the array period Λ = 400nm, the wavelength of the surface plasmons between the CL-GPR cavities is close to 2Λ, which means that surface plasmons leaked from the two neighboring cavities are approximately in antiphase, and this may reduce the efficiency of cavity coupling. Increasing the grating period to Λ = 600nm [Fig. 2(b)] results in more favorable interference conditions for the surface plasmons, which enhances the coupling between the cavities in the CL-GPR array.

In other words, the observed resonance for Λ = 600nm might be caused by a complex structural mode that is a combination of mutually transforming GSPs under the strips and surface plasmons between the strips, rather than just by GSPs under the individual strips [see also Fig. 6(d)]. Reducing thickness t of the SiO_2 layer results in reduced efficiency of leakage of the GSPs into the surface plasmons between the strips, and the structural resonance tends towards that of an individual CL-GPR [including the expected increase of resonant wavelength with decreasing t - Fig. 2(c)]). On the contrary, at relatively large values of t, efficient mutual transformation of gap and surface plasmons at the edges of the gold strips leads to the significant deviation of the resonance behavior from the expected trends for an individual CL-GPR. For example, this may cause the unexpected red shift of the resonant wavelength with increasing t, especially at the larger structural period Λ = 600nm ensuring more favorable interference conditions for the surface plasmons [the upper solid curve in Fig. 2(c)]. This effect is equivalent to increasing w' and decreasing n [Fig. 2 (c)].

The obtained results and interpretations can be further illustrated by the distributions of the electric field in CL-GPRs (Fig. 3 and Fig. 4). The presented electric field distributions clearly display the standing wave patterns for the GSP with a node under the center of the gold strip, as expected for the fundamental resonance mode. It is also evident that even for very thin SiO_2 layers the mode fields significantly extend beyond the edges of the gold strip [Fig. 3(a) and Fig. 4(a)], which is a confirmation of the above conclusion that the effective resonator length w' appears significantly larger than the width of the gold strip w. If the SiO_2 thickness is increased [e.g., to ~t = 70nm - Fig. 3(b) and Fig. 4(b)] the fundamental mode becomes practically delocalized and effectively spreads over the whole CL-GPR array. Importantly, this delocalization is stronger for the larger array period of 600 nm [Fig. 4(b)], which is probably the consequence of the discussed coupling of the CL-GPR cavities by means of surface plasmons in the gaps between the gold strips (see above). This delocalization of the fundamental CL-GPR mode in the x-direction at larger values of t is also demonstrated by the dependences of the normalized electric field in the middle of the SiO_2 layer as a function of the x-coordinate [Fig. 3(c) and Fig. 4(c)]. Despite the discussed delocalization of the fundamental CL-GPR mode (and thus efficient coupling between the CL-GPRs in the array), the electric field is still significantly localized within or near the thin SiO_2 layer [Fig. 3(b) and Fig. 4(b)]. Thus the delocalization caused by the cavity coupling occurs anisotropically and mainly along the dielectric layer, rather than in the direction perpendicular to it. This is a practically important aspect as it allows localization of the plasmonic resonantly enhanced field within a thin dielectric (semiconductor) layer, which could be a significant opportunity for increasing efficiency of photovoltaic devices and photodetectors.

#151634 - $15.00 USD Received 26 Jul 2011; revised 25 Aug 2011; accepted 7 Sep 2011; published 20 Sep 2011

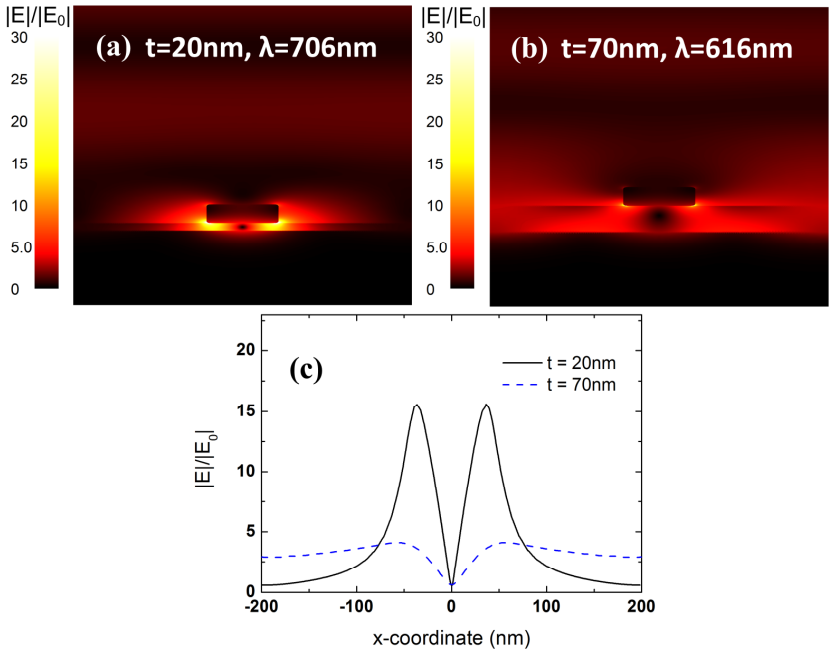

Fig. 3. Typical distributions of the resonant electric field magnitude in the (x,y)-plane for the two different SiO_2 thicknesses (a) t = 20nm and (b) t = 70nm in a periodic CL-GPR array with Λ = 400nm. (c) The dependences of the normalized (to the amplitude of the incident wave E_0) local electric field in the middle of the SiO_2 layer for Λ = 400nm; both the dependences were plotted for the resonant wavelengths of 706nm and 616nm for the respective values of t = 20nm and t = 70nm.

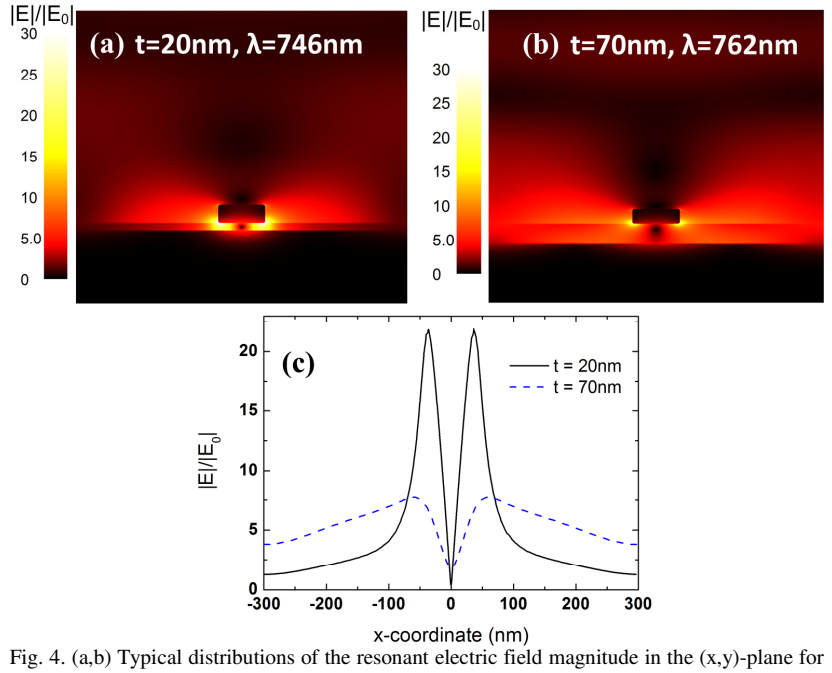

Fig. 4. (a,b) Typical distributions of the resonant electric field magnitude in the (x,y)-plane for the two different SiO_2 layer thicknesses (a) t = 20nm and (b) t = 70nm in a periodic CL-GPR array with Λ = 600nm. (c) The dependences of the normalized (to the amplitude of the incident wave E_0) local electric field in the middle of the SiO_2 layer for Λ = 600nm; both the dependences were plotted for the resonant wavelengths of 746nm and 762nm for the respective values of t = 20nm and t = 70nm.

#151634 - $15.00 USD Received 26 Jul 2011; revised 25 Aug 2011; accepted 7 Sep 2011; published 20 Sep 2011

3. Linear reflectivity measurements

The experimental investigation of CL-GPRs was conducted using several 30μm × 30μm periodic arrays - each consisting of 5 rows of 5μm long and 53nm thick gold nanostrips [Fig. 5(a,b)]. The separation between the neighboring rows of strips was 1μm [Fig. 5(a)]. The strip width w and the period Λ within each row were fixed for the same array, but different for different arrays. The nanostrip arrays were fabricated in a single-step lithography, followed by lift-off applied to a 3nm thick titanium adhesion layer and 50nm thick gold film, on a silicon wafer which was pre-coated by a 100nm thick gold film (gold underlay) and 23nm thick SiO_2 film, deposited by electron-beam deposition and RF-sputtering, respectively.

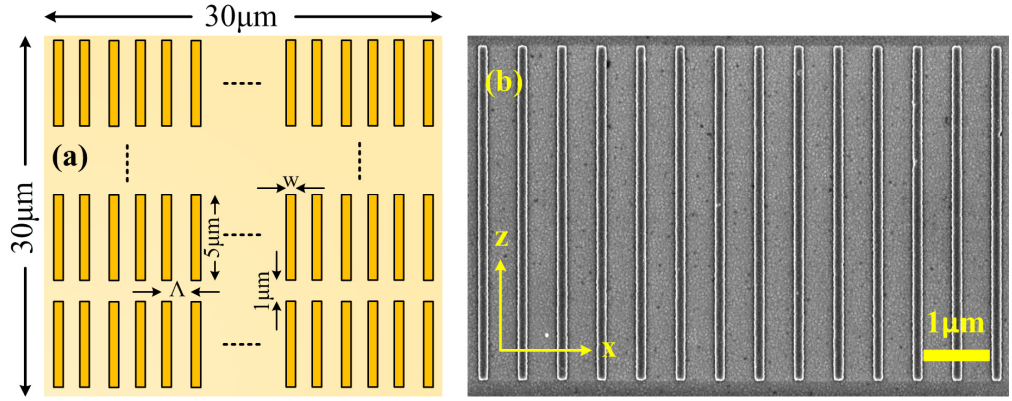

Fig. 5. (a) Schematic of the 30μm × 30μm CL-GPR array in the form of gold strips on a 23nm thick SiO_2 film and 100nm thick gold underlay. (b) A representative scanning-electron microscopy image showing a small section of a CL-GPR array with w = 135nm, h = 53nm, t = 23nm and Λ = 600nm.

In order to measure the reflectivity spectra, light from a broad band halogen light source was TM-polarized and subsequently focused by an objective, having 60x magnification and 0.85 numerical aperture, onto the 30μm × 30μm array. The reflected light was collected by the same objective, filtered spatially such that only the reflected light from the array was collected, sent through the analyzer (parallel to the polarizer) and finally collected by an optical fiber connected to a VIS/NIR spectrometer. The reflectivity from the array was normalized to the reflectivity from a similar-sized control patch of the continuous thick (100nm) gold underlay covered in the 23nm SiO_2 film with no gold strips forming CL-GPR arrays. The control patch was positioned close to the analyzed CL-GPR arrays to ensure approximately the same structural and material parameters as within the arrays.

The obtained experimental dependences of the measured normalized reflectivity from the CL-GPR arrays on vacuum wavelength are presented in Fig. 6(a,b) for the three different values of w = 85nm, 115nm and 135nm [Fig. 6(a)], and Λ = 400nm, 600 nm and 800 nm [Fig. 6(b)]. For comparison, reflectivity spectra are simulated with the same structural parameters as in the experiment [Fig. 6(c,d)]. All of the experimental curves for the TM polarization of the incident light display the expected resonant behavior associated with the excitation of GSPs in the gaps between the gold strips and the thick gold underlay, confirming the theoretical predictions for CL-GPRs. The wavelength positions of the experimentally observed GSP resonances [Fig. 6 (a,b)] are generally in a good agreement with the theoretical predictions [Fig. 6 (c,d)], albeit the experimentally observed resonances are consistently red shifted with respect to the calculated (without any fitting) ones. Fitting the simulated spectra by changing the structural parameters would further improve the agreement, but since the simulated reflectivity spectra contain the main important features of the experimental spectra, we decided not to do so. Figure 6(a) demonstrates that for a fixed array period (Λ = 600nm), the resonant wavelength increases with increasing width of the gold nanostrip [Fig. 6(a)]. This is in agreement with the understanding that the observed resonances are related to GSPs

#151634 - $15.00 USD Received 26 Jul 2011; revised 25 Aug 2011; accepted 7 Sep 2011; published 20 Sep 2011

in the gaps between the gold strips and the gold underlay. The observed red shift for the resonant wavelengths with increasing the array period Λ from 400nm to 600nm [the solid and dashed curves in Fig. 6(b,d)] is in agreement with the theoretically predicted increase of the effective CL-GPR length *w'* [Fig. 2(c)] and the discussed coupling between the CL-GPR cavities and possible interaction between the fundamental GSP resonance and the grating resonance (the Rayleigh anomaly). The reflectivity curve for the TE polarization of the incident light expectedly does not display any resonances in the structure and demonstrate rather featureless behavior at the level of ~96% - Fig. 6(a), which once again confirms the validity of the presented theoretical interpretation and analysis of these structures.

Figure 6(a) and Fig. 6(b) also suggest that there are optimal structural parameters such as period Λ and width of the strips *w* at which the reflectivity of the incident TM radiation from the structure may be close to zero due to nearly 100% coupling of this radiation into the fundamental CL-GPR mode [see the solid curve in Fig. 6(b) and the solid and dashed curves in Fig. 6(a)]. In particular, the obtained dependences [Fig. 6(a) and Fig. 6(b)] suggest that the separation between the neighboring gold strips may be one of the most important optimization parameters. For example, increasing strip width *w* at a fixed period Λ = 600nm (i.e., decreasing separation between the gold strips) results in increasing strength of the CL-GPR fundamental resonance [Fig. 6(a)]. Similarly, decreasing period Λ at a fixed width *w* = 85nm (i.e., again decreasing separation between the gold strips) also results in increasing strength of the CL-GPR fundamental resonance [Fig. 6(b)]. Optimal separation between the strips may be expected to ensure the optimal coupling efficiency of the incident radiation into the fundamental mode of CL-GPRs, leading to the nearly 100% absorption of the incident radiation.

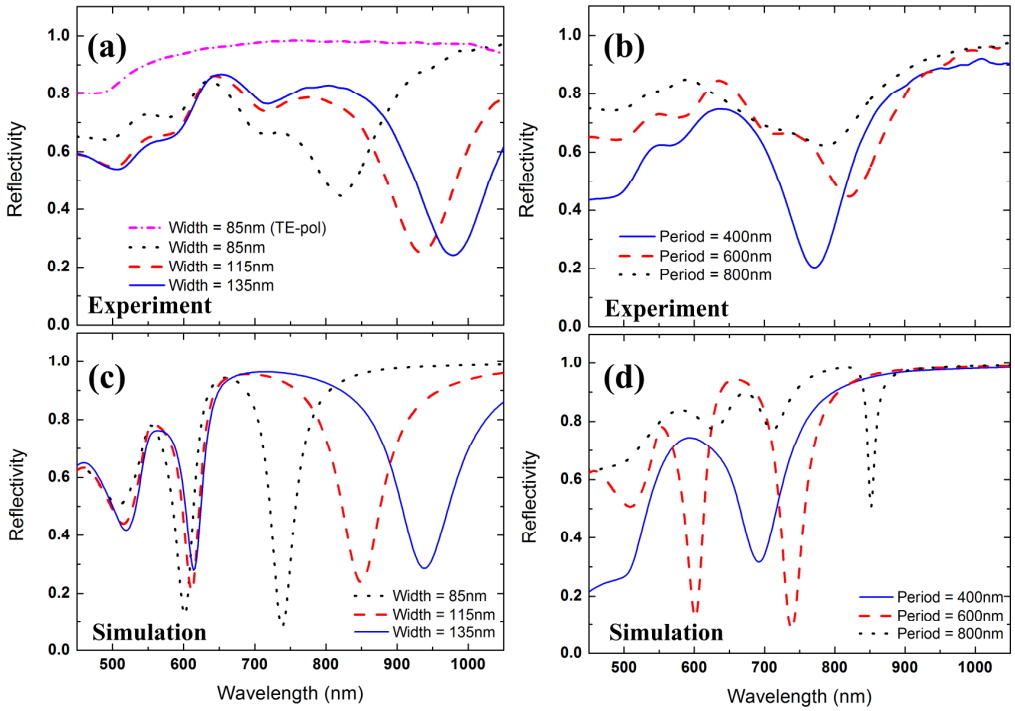

Fig. 6. Experimental (a,b) and simulated (c,d) reflectivity spectra from the CL-GPR arrays for the normally incident beam with the TM polarization: (a,c) fixed Λ = 600nm and three different strip widths *w*, and (b,d) fixed *w* = 85nm and three different array periods Λ. The dash-and-dot curve in (a) shows the reflectivity spectrum for a normally incident focused beam with the TE polarization.

The Rayleigh anomaly (the grating resonance) is not clearly seen in the experimental spectra for Λ = 600nm, which could be explained by the fact that we used a high numerical

#151634 - $15.00 USD Received 26 Jul 2011; revised 25 Aug 2011; accepted 7 Sep 2011; published 20 Sep 2011

aperture in order to strongly focus radiation from the halogen light source (achieving the spot size of ~80μm) instead of the normally incident plane wave in the simulation (see also [26]). This might also be one of the reasons for the fact that the experimentally obtained reflectivity minimum for Λ = 600nm is less pronounced than for Λ = 400nm [the solid and dashed curves in Fig. 6 (b)], which is the opposite tendency compared to the theoretical predictions [Fig. 6 (d)].

The theoretically predicted Q-factors for the fundamental CL-GPR resonance are up to ~20 when Λ = 600nm, which is close to the quasistatic limit [31]. For Λ = 400nm the theoretically predicted Q-factors are ~8, which is comparable with the experimental value of ~6.

4. Scanning two-photon luminescence microscopy

The predicted enhancement of the electric field was ~22 in the middle of the SiO_2 layer for Λ = 600nm [Fig. 4(c)] i.e., larger than for Λ = 400nm - Fig. 3(c). However, the experimentally observed fundamental CL-GPR resonance was stronger at Λ = 400nm and, therefore, the field enhancement is expected to be larger for Λ = 400nm. The local field intensity enhancements $(|E|/|E_0|)^2$ in the CL-GPR arrays were evaluated experimentally using the scanning two-photon luminescence (TPL) microscopy whose experimental setup was described for the enhancement measurements for resonances in gold strips [32], split-ring resonators [33], gold disk fractal patterns [34,35], and tapered periodic slits in gold [36]. To measure TPL from the CL-GPR arrays, the first harmonic (FH) wavelength of a pulsating mode-locked Ti-Sapphire laser was used with ~200fs pulse, ~80MHz repetition rate, fixed average incident power of ~0.1mW, and tight focusing (spot size ~0.8μm) by means of a Mitutoyo infinity-corrected (x100, numerical aperture 0.70) objective. The reflected FH and TPL were concurrently collected by the same objective and by using a scanning computer-controlled translation stage with the 200nm step size and accuracy of ~4nm a 10μm × 10μm region partly overlapping with a CL-GPR array was scanned. The FH- and TPL signals were separated by the appropriate filters and detected by photomultiplier tubes (PMTs). The PMT for detection of the TPL signal was connected to a photon counter with ~10 dark counts per second (cps) and the integration time of 100ms. As for the linear reflectivity measurements [Fig. 6(a,b)], the polarizer and analyzer were both aligned perpendicular to the nanostrips.

The typical FH and TPL images at the wavelength 760nm are shown in Fig. 7(a) and Fig. 7(b), respectively. The corner of a CL-GPR array is seen as the black region [Fig. 7(a)] and the bright (yellow) region [Fig. 7(b)] in the FH and TPL images. The x-dependence of the FH signal [Fig. 7(c)] clearly shows that the FH-reflectivity is low inside (~0.2) and high outside (~0.9) the array. These values are in good agreement with the reflectivities obtained by means of the broadband light source. The TPL dependence in Fig. 7(c) features high contrast with the strong signal with the average of ~350 cps inside the array, and nearly zero outside the array. This confirms that the CL-GPR arrays significantly localize and enhance light intensity compared to the control patch with no gold strips [the black region in Fig. 7(b)].

In order to estimate the intensity enhancement as a function of wavelength, TPL scanning was conducted for the wavelengths between 730nm and 820nm in 10nm wavelength steps. The intensity enhancement factor α can be estimated for each wavelength via the expression [37]:

$$\frac{TPL_{array}}{TPL_{ref}} = \alpha^2 \frac{\left\langle P_{array} \right\rangle^2 A_{array}}{\left\langle P_{ref} \right\rangle^2 A_{ref}}, \tag{3}$$

where TPL_{array} is the average TPL signal per one pixel (i.e., one scanning step), obtained from the ~6μm × 4μm region inside the CL-GPR array [bright region in Fig. 7(b)], $\left\langle P_{array} \right\rangle$ is the average power of ~0.1mW in the focal spot during scanning, A_{array} is the area with the

#151634 - $15.00 USD Received 26 Jul 2011; revised 25 Aug 2011; accepted 7 Sep 2011; published 20 Sep 2011

locally enhanced fields within a region whose area is equal to A_{ref} that is the area of the focused FH

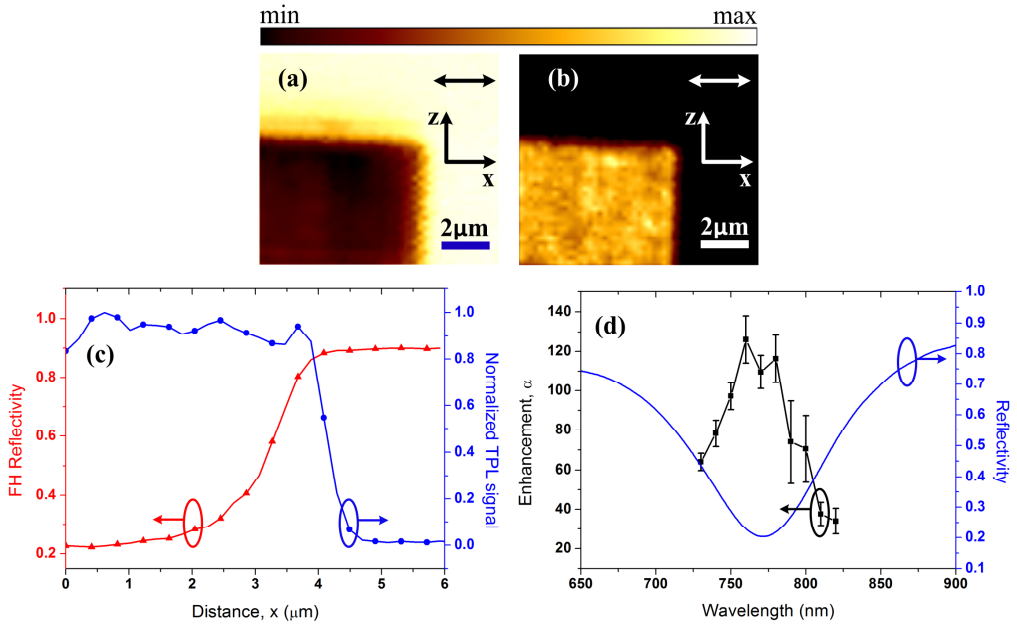

Fig. 7. Typical FH (a) and TPL (b) images near the corner of a CL-GPR array with w = 85nm and Λ = 400nm; the polarization of the incident beam is in the x-direction. (c) The typical measured x-dependencies of the FH reflectivity and normalized TPL signals along the x-direction across the array edge at x~4μm. (d) The estimated intensity enhancement factor α as a function of the incident wavelength, superimposed with the measured reflectivity spectrum.

spot (typically, $A_{array} < A_{ref}$), TPL_{ref} is the average TPL signal per one pixel, obtained from scanning a 2μm × 2μm reference patch of the smooth continuous gold film of 50nm thickness (deposited onto the same structure and in the same process as the CL-GPR gold strips), $\langle P_{ref} \rangle^2$ is the average power between 4mW and 8mW (depending on the wavelength) in the focal spot during scanning of the reference patch of smooth gold film.

As it is difficult to evaluate A_{array} and the coupling of TPL from the structure to free space without comprehensive theoretical investigations, the enhancement factor α [Eq. (3)] should be understood as a measure of average enhancement in the structure as compared to smooth gold. In this particular case the enhancement factor α was estimated under the assumption: $A_{array} = A_{ref}$. The resultant experimental dependence of α on wavelength is shown in Fig. 7(d) and demonstrates excellent agreement of the enhancement maximum with the minimum of the measured reflectivity spectrum for the CL-GPR array with Λ = 400nm - both occurring at the same incident wavelength of 760nm [Fig. 7(d)]. Because TPL is a surface-sensitive technique, the reflectivity minimum coinciding with the enhancement maximum is important as this verifies that the estimated enhancement is caused by the local intense fields in CL-GPRs, rather than by surface roughness or other irregularities. It is also important to note that the assumption $A_{array} = A_{ref}$ (instead of the actual $A_{array} < A_{ref}$) results in a likely underestimate of the obtained experimental value of α ~126. This is in agreement with the theoretical predictions of larger intensity enhancements of ~225 [Fig. 3(c)].

#151634 - $15.00 USD Received 26 Jul 2011; revised 25 Aug 2011; accepted 7 Sep 2011; published 20 Sep 2011

5. Conclusions

In summary, we have demonstrated numerically and validated experimentally efficient resonant excitation of GSPs in the CL-GPR structures formed by gold nanostrips (fabricated by single-step lithography) on a continuous SiO_2 film on a thick gold underlay. The possibility of nearly 100% resonant absorption of the incident TM radiation due to its efficient coupling into the fundamental CL-GPR mode was demonstrated theoretically and confirmed experimentally for thin SiO_2 films with the thickness of ~10 - 20nm. Though obtained for the retardation-based resonances involving GSPs, the theoretically predicted Q-factors for the fundamental CL-GPR modes were shown to be close to the quasistatic limit [31]. The measurements using the scanning TPL microscopy confirmed major local field enhancement in the considered structures.

We have presented detailed physical interpretations of the obtained results, elucidating the crucial role of GSPs in plasmonic structures with finite-size metal strips placed on an extended multilayer structure and developing a general resonator model that can be applied to GPRs. The developed physical interpretation can be used to account for previous observations [25–27], providing also simple design guidelines for further experiments. Thus, for example, the localized plasmon resonance observed in a recent study [27] at the wavelength of 1050nm can directly be related to the fundamental GPR mode, and its resonant wavelength can be evaluated (within 5%) using the developed resonator model [Eq. (2)] with a typical value of the phase parameter $n = 1/3$ (taking also into account the GSP dispersion for given configuration parameters and material constants).

The localization of the significant portion of the enhanced local field inside the thin dielectric layer opens excellent opportunities for using the considered CL-GPR arrays to increase efficiency of photovoltaic devices and design photodetectors with enhanced signal-to-noise ratio. The CL-GPR structures with the obtained high Q-factors can also form an efficient and cost-effective basis for other plasmonic applications such as nano-optical sensors and surface-enhanced Raman spectroscopy techniques, including single-molecule detection and identification.

Acknowledgements

We acknowledge financial support for this work from the VELUX Foundation and from the Danish Council for Independent Research (the FTP project ANAP, contract no. 09-072949).

#151634 - $15.00 USD Received 26 Jul 2011; revised 25 Aug 2011; accepted 7 Sep 2011; published 20 Sep 2011